https://doi.org/10.5194/amt-2024-124
Preprint. Discussion started: 5 August 2024

Atmospheric Measurement Techniques Discussions

Cloud phase estimation and macrophysical properties of low-level clouds using in-situ and radar measurements over the Southern Ocean during the SOCRATES campaign

Anik Das[1], Baike Xi[1], Xiaojian Zheng[2], and Xiquan Dong[1]*

[1]Department of Hydrology and Atmospheric Sciences, University of Arizona, Tucson, AZ, USA

[2]Environmental Science Division, Argonne National Laboratory, Lemont, IL, USA

Correspondence: Xiquan Dong (xdong@arizona.edu)

Abstract. The Southern Ocean (SO) provides a unique natural laboratory for studying cloud formation and cloud-aerosol interactions with minimal anthropogenic influence. The Southern Ocean Clouds, Radiation, Aerosol Transport Experimental Study (SOCRATES), was an aircraft-based campaign conducted from January 15 to February 28, 2018, off the coast of Hobart, Tasmania. During SOCRATES, the NSF/NCAR GV research aircraft, equipped with in-situ probes and remote sensors, observed aerosol, cloud and precipitation properties, and provided detailed vertical structure of clouds over the SO, particularly for the low-level clouds (below 3 km). The HIAPER Cloud Radar (HCR) and in-situ cloud and drizzle probes (CDP and 2DS) measurements were used to provide comprehensive statistical and phase-relevant macrophysical properties for the low-level clouds sampled by the 15 research flights during SOCRATES. A new method based on HCR reflectivity and spectrum width gradient was developed to estimate cloud boundaries (cloud-base and -top heights) and classify cloud types based on their top and base heights. Low-level clouds were found to be the most prevalent, with an almost 90% occurrence frequency. A new phase determination method was also developed to identify the single-layered low-level clouds as liquid, ice, and mixed-phases, with occurrence frequencies of 45.4%, 32.5%, and 22.2%, respectively. Low-level clouds over the SO have significantly higher SLW concentrations, with liquid being most prevalent at higher temperatures, ice phase dominating at lower temperatures, and mixed phase being least common due to its thermodynamic instability. Regarding their vertical distributions, the liquid phase occurs most frequently in the lower mid-cloud range (from 500 m to 1 km), the mixed phase dominates at cloud bases lower than 1 km but is well distributed along the vertical cloud layer, while the ice phase is prevalent from the middle to upper cloud levels (1-3 km). The higher occurrence of the mixed phase at the cloud base could be attributed to large drizzle-sized drops and/or ice particles.

1 Introduction

Southern Ocean (SO) clouds impact the radiation budget over the region in a significant manner (Kay et al., 2012; McCoy et al., 2014) which the global climate models cannot simulate accurately (Bodas-Salcedo et al., 2016; Cesana & Chepfer, 2013; Kay et al., 2016; Trenberth & Fasullo, 2010; Wang et al., 2018), which tends to underestimate the shortwave fluxes, also producing lower cloud fraction and less supercooled liquid water than observed (D'Alessandro et al. 2021). The SO represents a remote, pristine, and pre-industrial environment (Hamilton et al., 2014; Uetake et al., 2020; Humphries et al., 2021) and provides a unique natural laboratory to understand cloud formation and microphysical properties, cloud-aerosol interactions with minimal anthropogenic influences (McCoy et al., 2015; Xi et al., 2022).

The low-level SO clouds feature a predominantly high concentration of supercooled liquid water (SLW, almost 80% of low-level clouds contain SLW over a temperature range of -40 to 0^{o}C, Hu et al., 2010). Their cloud macrophysical and microphysical properties are different from subtropical marine boundary layer (MBL) clouds which contain almost all liquid clouds (Dong et al., 2014; Wu et al., 2020; Zhao et al., 2020) and from the Arctic mixed-phase clouds with a top layer of liquid and bottom layer of ice clouds (Qiu et al., 2015). Understanding the dominant cloud phase and phase-related spatial homogeneity of the low-level SO clouds is crucial to expanding our current understanding of the region along with developing better parametrization for the increased accuracy of the global climate model predictions (Zhao et al, 2023; Liu et al 2023; etc.). Identifying the cloud phase is crucial to accurately retrieving cloud macrophysical and microphysical properties because most algorithms are tuned for specific cloud phases over different climatic regions (Shupe, 2007). Incorrect parametrization of low-level clouds is a key climate uncertainty and bias; and causes wide intermodel variation (~50%) (Klein et al., 2017) as liquid-to-ice conversion of cloud particles reduces albedo at the top of the atmosphere (TOA) (Xi et al., 2022).

Several studies exist on classifying cloud-type, cloud phase and hydrometeor-type detection over the SO region (e.g., Xi et al., 2022; Desai et al., 2023; D'Alessandro et al., 2021, 2019; Romatschke & Vivekanandan., 2023; Atlas et al., 2021; Schima et al., 2022; Zaremba et al., 2020) and Arctic clouds (e.g. Shupe 2007; Korelov & Milbrandt, 2022). They utilized a suite of in-situ, radar-lidar and machine-learning approaches to predict cloud phase or cloud-hydrometeor types along with their relevant macro- and micro-physical properties but reported a significant difference in phase retrieval results and phase transition processes based on the nature of the campaign and instrumentation. These studies have various performances depending on their retrieval methods and assumptions during retrievals. Xi et al. (2022) used the W-Band radar measurements and microwave radiometer retrieved cloud liquid water path (LWP) to estimate cloud phase and macrophysical properties over the SO (North of 60º and South of 60º latitude) for clouds sampled during the ship-based the Measurements of Aerosols, Radiation, and Clouds over the Southern Ocean (MARCUS, Xi et al., 2022; Marcovecchio et al., 2023; McFarquhar et al., 2016, 2021) campaign and estimated a greater frequency of mixed-phase clouds followed by ice and liquid clouds. Ship-based measurements during the MARCUS can provide accurate cloud boundaries and their vertical distributions. Wang & Sassen (2001) presented algorithms for retrieving cloud macrophysical properties, such as boundary, thickness, phase, type, and precipitation, using a combination of ground-based lidar, millimeter-wave radar, IR radiometer, and MWR measurements at the ARM SGP CART site in Northern Oklahoma. Further, Shupe (2007) provided an array of ground-based Lidar-Radar threshold values to estimate cloud hydrometeor phase including aerosols, liquid, mix, ice, drizzle and rain designed for the study of Arctic clouds. Compared to the ground-based measurements, the aircraft in situ measurements, however, can provide more reliable datasets without the issues of retrieval methods and assumptions because aircraft can fly in greater proximity to the cloud boundaries and even inside the cloud layers. Also, the onboard radar and lidar suffer less attenuation than the ground-based remote sensors (Ewald et al., 2021).

The Southern Ocean Clouds, Radiation, Aerosol Transport Experimental Study (SOCRATES) aircraft field campaign provided a valuable dataset to investigate the MBL clouds over the SO. The SOCRATES was an aircraft-based campaign that used the National Science Foundation (NSF)/National Center for Atmospheric Research (NCAR) Gulfstream-V (GV) research aircrafts based out of the coast of Hobart, Tasmania (42-62°S and from 133°-163°W) from 15 January to 28 February 2018, targeting cold sector boundary layer clouds and airborne sampling of in-, below- and above-cloud transects obtaining both time series and vertical cloud information using an array of in-situ cloud and drizzle sampling probes and radar-lidar instruments, mostly spanning a period of midnight to early morning for each flight track on subsequent days. The in-situ probes and remote sensors (cloud lidar and radar) onboard the aircraft flown during the SOCRATES campaign provide a direct observation of precipitation, cloud particles, and aerosols below, inside and above the cloud layers sampled, along with vertical profiles, for a better characterization of the MBL structure and free troposphere. D'Alessandro (2021) used the suite of in-situ cloud and drizzle sampling probes (CDP & 2DS) onboard the NCAR-GV aircraft during SOCRATES to estimate cloud phase heterogeneity and frequency distributions predicting significant SLW and ice phase concentrations using a multinomial logistical regression model (MLR). Romatschke and Vivekanandan. (2023) used a fuzzy logic scheme to classify cloud hydrometeor type as a time-height profile using an array of cloud radar-lidar derived values.

According to Wang et al. (2012), integrating in-situ sampling capabilities with remote sensing measurements offers significant advantages for studying atmospheric processes. In this context, the integrated 2-dimensional cloud profiles obtained through remote sensing of microphysical processes

https://doi.org/10.5194/amt-2024-124
Preprint. Discussion started: 5 August 2024

complement the detailed size-resolved distributions captured by in-situ cloud measurements. Therefore, solely relying on either in-situ or remote sensing measurements can lead to certain disagreements in cloud profile as the sampling probes can only detect cloud particles at the flying altitude while the remote sensing profiles can provide vertically resolved cloud profile but with an offset of around 100-200 meters. The lidars have a smaller operating wavelength compared to radar and provides well-resolved vertical profiles for detecting aerosols, optically thin clouds and cloud boundaries, (Wang et al., 2012, 2009; McGill et al., 2002) but its signals are easily attenuated by optically thick clouds, such as liquid clouds (Sassen., 1991) as observed over the SO. Therefore, we exclusively used radar measurements to estimate cloud boundaries and cloud phase for optically thick clouds in this study. Furthermore, we also tune the High Spectral Resolution Lidar (HSRL) measured Particle Depolarization Ratio (PLDR) thresholds based on the phase estimation method presented in this study. This adjustment was seen necessary because the existing PLDR thresholds presented in Sassen (1991), Intrieri (2002), and Shupe (2007) were developed for Arctic clouds, which differ significantly from the low-level clouds over the Southern Ocean (SO).

In this study, we aim to use a combination of both in-situ and radar-based measurements during SOCRATES to develop a new method to classify the MBL cloud phase and determine cloud boundaries over the SO for low-level clouds. The newly developed classification method can be used to help answer the following scientific questions:

1. What are the dominant cloud types, their associated cloud phase, base and top heights, and their vertical distribution?

2. What are the phase-specific macrophysical properties for SO low-level clouds sampled during the SOCRATES campaign?

The paper is organized in the following manner: data and methods are introduced in Section 2. The statistical results for all cloud properties during the SOCRATES campaign are presented in Section 3. Cloud phase-specific results and comparisons with other algorithms for the low-level clouds are discussed in Section 4, and finally, Conclusions and Summary are given in Section 5.

2 Data and methods

2.1 SOCRATES aircraft campaign

The Southern Ocean Clouds, Radiation, Aerosol Transport Experimental Study (SOCRATES) aircraft field campaign was conducted over the SO with a total of 15 research flights from 15 January to 28 February 2018 (McFarquhar et al., 2021). During SOCRATES field campaign, the Cloud Droplet Probe (CDP) and 2-dimensional stereo- particle imaging probe (2DS) were utilized to measure cloud and drizzle microphysical properties, respectively. Additionally, HCR and HSRL were installed on the RV aircraft to detect cloud structure, phase and boundaries (McFarquhar et al., 2021). HSRL particle linear depolarization ratios (PLDR) were widely used as a screening tool for cloud phase determination with liquid clouds having PLDR less than 0.11, mixed-phase clouds falling between 0.11 and 0.15, and ice clouds having PLDRs greater than 0.15 (Shupe et al., 2005; Xi et al., 2022). The 2DS in-situ measurements serve as an additional screening to eliminate the ice particles (D>200 μm). More instrumental details about the SOCRATES campaign can be found in McFarquhar et al. (2021).

The suite of in-situ probes and radar-lidar instruments onboard the SOCRATES aircraft is listed in Table 1, along with their detection limits and uncertainties. The particle size distribution and number concentration were retrieved from the CDP and 2DS microphysical probe measurements and merged

https://doi.org/10.5194/amt-2024-124
Preprint. Discussion started: 5 August 2024

Atmospheric Measurement Techniques
Discussions

to create one continuous dataset with size bins from 2 to 40 µm corresponding to cloud droplets and 40 µm above for drizzle particles (to 1280 µm), at a 1 Hz temporal resolution for each research-flight. Reflectivity (dBZ), Doppler Velocity (V_d) (m/s), and Spectrum Width (WID) (m/s) were retrieved from the original 2 Hz temporal resolution of the HCR radar measurements and were averaged to match the 1 Hz frequency resolution of the in-situ probes and further interpolated to fixed radar-heights at a range gate of 19.2 meters. The same treatment was done for the HSRL-retrieved Backscatter Coefficient β ($m^{-1}sr^{-1}$) and Particle Linear Depolarization Ratio (PLDR) (unitless). The HSRL (lidar) signal is highly sensitive to greater cloud droplet concentrations and can be attenuated within a few hundred meters in liquid cloud layers (Ewald et al., 2021; Sassen, 1991). Thus, it is not used for phase or boundary estimation in optically thicker MBL clouds discussed in this paper. The atmospheric temperature (°C) for the cloud samples was retrieved from the 2-dimensional ERA5 reanalysis product, which is available in the HCR-HSRL merged dataset at the EOL data archive. This dataset matches the vertical and temporal resolution of the HCR-HSRL data (NCAR/EOL HCR Team., 2023). Temperatures below -40 oC are not considered during further analysis as they represent homogenous freezing temperatures (majorly all ice) and most mixed phases exist only over the range of -40 to 0 ºC (e.g., Shupe et al., 2007). The dataset is further filtered to keep only the nadir or zenith pointing direction of the HCR-HSRL merged dataset, all the in-transition or rotational pointing directions (which were not equal to ±90 degrees) were removed. The 2DS particle morphology or habit imagery data (Wu and McFarquhar., 2019) was also retrieved and visualized using the Illinois/ Oklahoma Optical Probe Processing Software (XPMS2D, UIOOPS, McFarquhar et al., 2018).

Table 1. Measurements from specific instruments used in this study and their relevant properties.

	INSTRUMENT	MEASUREMENT	Size Range/Resolution	Uncertainties	REFERENCES
In-Situ Probes for Bulk Cloud Sampling	Cloud Droplet Probe **(CDP)**	Size distribution and concentration of hydrometeors with a diameter between 2-50 µm	2-50 µm	Cannot resolve non-spherical particles accurately	Lance et al., 2010
	Two-Dimensional, Stereo, Particle Imaging Probe **(2D-S)**	Size distribution and concentration of hydrometeors with a diameter between 10 to 1280 µm range	10-µm D>40 µm for all particles D> 200 µm for ice	Cannot resolve for particle sizes D <50 µm, also ice particle detection is certain only for D>200 µm.	Lawson et al., 2006; 2008 Baker et al., 2009 Wu and McFarquhar., 2019
Radar-Lidar remote sensors	HIAPER Cloud Radar **(HCR)**	Reflectivity, Doppler Velocity, Spectral Width, Linear Depolarization Ratio (LDR), etc.	~19 m in vertical resolution Frequency: 94.40 GHz	Attenuates for larger particle sizes	NCAR/EOL HCR Team., 2014 Romatschke et al., 2021 Vivekanandan et al., 2015
	High Spectral Resolution Lidar **(HSRL)**	Backscatter Coefficient, Particle Linear Depolarization Ratio (PLDR), Extinction Coefficient, etc.	Wavelength: 532 nm	Sensitive to optically thin cloud layers	NCAR/EOL HSRL Team., 2012 Eloranta., 2005

2.2 Estimation of cloud boundaries

There are multiple existing methods of estimating cloud base and top heights, for example, using thresholds for lidar returned power, depolarization, or backscatter (e.g., Intrieri et al., 2002; Kang et al., 2021, 2024) or thresholding in-situ measured vertically resolved liquid water path (LWP) or liquid water content (LWC) and cloud droplet number concentration. For this study, the cloud base was estimated as the lowest height (from the sea surface) where the HCR Spectrum Width (WID) Gradient is the lowest in value (or highest negative gradient). The lowest WID gradient indicates the change from a precipitation layer to the cloud layer where the gradient of spectrum width decreases sharply. The cloud-base height (H_{base}) was also estimated using the HSRL backscatter coefficient threshold, but this cloud-base height was found to be around 400 m higher than that derived from HCR spectrum width gradient. Higher spectrum width around the cloud base indicates a greater turbulence and wider range of particle velocities observed which correlate to potentially stronger turbulence, and likely drizzle or precipitation. This argument is further improved by the aircraft in situ measured microphysical properties.

The cloud-top height (H_{top}) is measured as the highest height (from the cloud base) where prominent HCR reflectivity (dBZ >-50) is observed following the method of Kang et al. (2024). Finally, cloud thickness (ΔH) is estimated as the difference between cloud-top and -base heights, $\Delta H = H_{top} - H_{base}$. For double-layered clouds, each single-layer cloud-base and -top heights were identified separately but are not reported in this study as only single-layered cloud types were used for further analysis. The accuracy of the estimated cloud-top and -base heights for the low clouds have been verified by mapping them on the radar detected cloud profile (Fig. 1.) and will be discussed in following sections. This method of estimating H_{top} and H_{base} can be used to find cloud boundaries in the absence of a readily available radiosonde or dropsonde measured cloud heights dataset.

A case study for the retrieved cloud boundaries using the HCR reflectivity and spectrum width gradient is illustrated in Fig. 1(a-d). Using the spectrum width gradient for estimating cloud-base heights allows finding cloud and drizzle base above the precipitating layer with minimal errors compared to lidar HSRL-Backscatter values which attenuate faster for thicker cloud layers. Boundary estimation was carried out for each sublayer separately for double-layered clouds (not shown). Isolated cloud transects less than 50 meters in vertical height and 10 seconds in temporal width (which appear as small, isolated dots or patches of reflectivity or spectrum width profiles in the following plot) are ignored as noise.

https://doi.org/10.5194/amt-2024-124
Preprint. Discussion started: 5 August 2024

Atmospheric Measurement Techniques Discussions

196
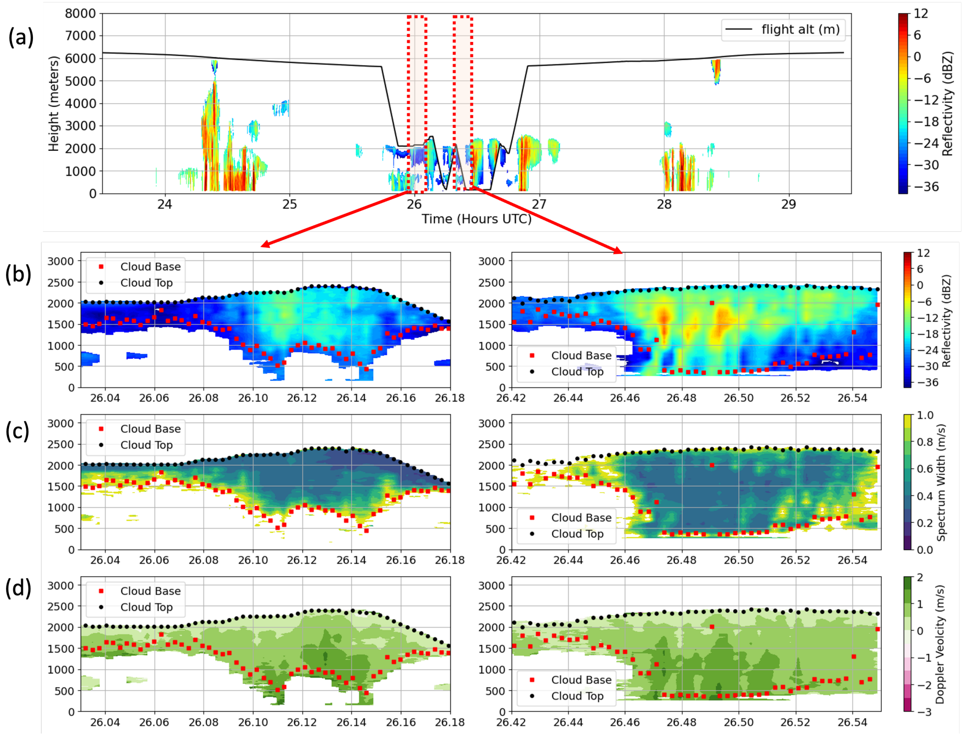

197 **Figure 1. (a) HCR Reflectivity (dBZ) profile for the entire flight track for RF01 from 23:30 UTC**
198 **(15 Jan 2018) to 05:30 UTC (16 Jan 2018). The solid black line in (a) indicates the flight altitude**
199 **in meters. The two red boxes in (a) are the subsection for which the cloud-top and -base heights**
200 **are displayed (b), (c), and (d). The left panels represent the cloud profiles when the flight was**
201 **flying above the cloud top and radar pointed nadir, while the right panel shows a zenith-pointing**
202 **radar cross-section with the flight flying below the cloud base. (b), (c), and (d) are the profiles of**
203 **HCR reflectivity, spectrum width (WID) and Doppler Velocity (V_d) with the cloud tops (black**
204 **squares) and cloud bases (red squares).**

205 **Table 2. Cloud classification using Base and Top heights.**

CLOUD TYPE	**CLASSIFICATION METHOD**
LOW (low-level clouds)	$H_{top} \leq$ 3km, in a single layer
MID (middle level)	$H_{base} >$ 3km and $H_{top} \leq$ 6km, in a single layer
HGH (high clouds)	$H_{base} >$ 6km, in a single layer
MOL (mid-over-low)	$H_{base} <$ 3km and $H_{top} \leq$ 6km, may not be single layer
HOM (high-over-middle)	3km<H_{base}<6km, and H_{top}>6km, may not be single layer
HML (high-over mid and low)	H_{base}<3km, and $H_{top} \geq$ 6km, extend over the whole tropospheric layer

https://doi.org/10.5194/amt-2024-124
Preprint. Discussion started: 5 August 2024

Atmospheric Measurement Techniques Discussions

2.3 Classification of Cloud type

After estimating the cloud-base, -top heights, and cloud thickness (H_{base}, H_{top}, ΔH), the cloud types are categorized following a classification method described by Xi et al., 2010, and summarized in Table 2. A single layer means that there is no other cloud layer above or below the classified cloud layer for the time series.

Based on this classification method, a significant number of LOW (H_{top} ≤3km) clouds were identified followed by MOL (H_{base} < 3km, H_{top} ≤6km) and MID (H_{base} > 3km, H_{top} ≤6km). Some HGH (H_{base} > 6km), HOM (3km<H_{base}<6km, and H_{top}>6km), and HML (H_{base}<3km, and H_{top} ≥ 6km) cloud types were also identified but almost insignificant or negligible in number relative to LOW, MID, and MOL types. Only a couple of flights had single or double-layered clouds with H_{base} and/or H_{top} > 6km, which were ignored to optimize for statistical deviation and minimize errors. Notice that these results are due to the selected cloud cases during the flight, which may not represent all the true cloud types.

Cloud phase estimation was only carried out for the single-layered LOW cloud type, which was the predominant cloud type during the SOCRATES field campaign. The statistical results for the predominant cloud types of LOW, MID and MOL are further discussed in Section 3.

2.4 In-Cloud Conditions

The cloud-droplet number concentration and particle size from the merged CDP+2DS dataset is used to calculate a continuous liquid water content (LWC) in g/m^3 for cloud and drizzle particles, using the equation (Kang et al., 2021; Zheng et al., 2024) as follows:

$$\mathrm{LWC} = \frac{4}{3}\,\pi\,\rho_w \sum_{\{i=1\}}^{\{n\}} r_i^3 \,.\, N_i, \qquad (1)$$

where ρ_w is the density of liquid water, r_i is the particle radius measured as droplet size distribution from the CDP+2DS particle size bins, and N_i is the number concentration (#/cm^3) per bin. The LWC values are further used to compute the liquid water path (LWP) in g/m^2 as a function of cloud thickness (ΔH) (Oh et al., 2018), as follows:

$$LWP = \sum_{\{j=1\}}^{\{n\}} LWC_j \,.\, \Delta H_j. \qquad (2)$$

The in-cloud conditions were constrained to keep cloud samples only containing LWC greater than 0.001 g/m^3, to remove noise or uncertainty in measurements. CDP number concentration less than 1 cm^{-3} corresponds to ice phase observations in particles with size less than 50 µm, and greater than or equal to 1 cm^{-3} corresponds to the liquid phase (D'Alessandro et al., 2021). Hence, choosing LWC threshold is based on the decision to ensure a significant cloud density and cloud number concentration, and remove clear-sky conditions or noise from aerosols. The number concentration of ice particles with diameters greater than 200 µm is very low (Zheng et al., 2024), as shown in Fig. 2, indicating that most ice phase particles occur below the 2DS-defined threshold of 200 µm for ice particle size distribution (Wu and McFarquhar, 2019).

https://doi.org/10.5194/amt-2024-124
Preprint. Discussion started: 5 August 2024

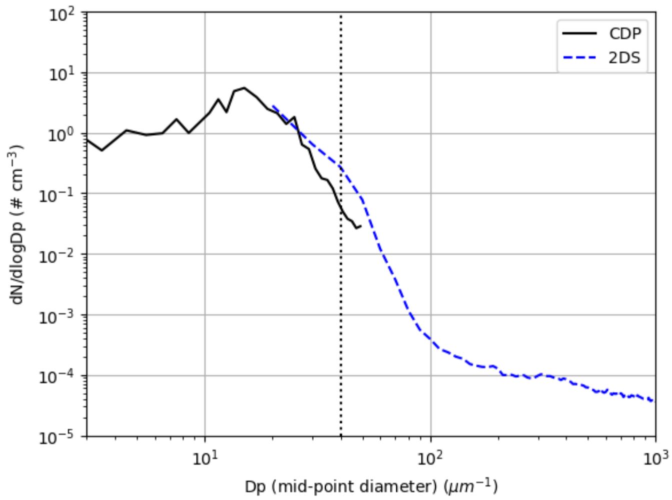

Figure 2. Cloud and Drizzle (CDP+2DS) size distributions aggregated for the 15 research flights during SOCRATES. The dashed line at D_p = 40 µm denotes the separation from cloud to drizzle droplets.

There is a small offset in the calculated LWP because LWC is derived from in-situ cloud (CDP) microphysical properties while cloud thickness is derived from the HCR and HSRL measurements. However, the difference was insignificant when these results were compared to the average LWP values observed over the SO by previous studies like Xi et al. (2022) and Mace et al. (2021). Future work could be done on finding the LWC and LWP as a function of the cloud vertical height profiles matched to the HCR-HSRL profiles, following the methods mentioned in Vivekanandan et al. (2020). Ice water content (IWC) in g/m^3 was also retrieved from the 2DS dataset for particle sizes ≥ 200 µm. The 2-dimensional HCR-HSRL parameters were further constrained for the cloud base and top heights for the classified cloud types in the vertical dimension and for the LWC threshold in the time dimension. The 2-dimensional air temperature (°C) from ERA5 was filtered to extract the cloud-base and -top temperatures. The aircraft-measured air temperature is not used in this study as it only measures temperature at the fixed flying altitude of the aircraft.

3 Statistical results for prominent cloud types

The most prominent cloud types identified using the cloud boundary estimation discussed in the Section 2.3, such as LOW, MID, and MOL, which are consistent of ~ 85-90% occurring frequencies in total from the 15 research flights during SOCRATES. Figure 3 summarizes the occurrence frequencies of the classified single-layered LOW, MID, and MOL clouds along with their vertical structures or the thickness (in km). Multilayered clouds were not considered for this classification due to their negligible occurrence frequencies compared to the single-layered clouds. LOW clouds are the most observed cloud type (~90%) compared to the other two cloud types (less than 10%), due to the nature of sampling and targeted cloud sector of the SOCRATES campaign. Most of the research flights flew below 6-7 km over the SO studying MBL clouds with greater amount of SLW (Schima et al., 2022).

https://doi.org/10.5194/amt-2024-124
Preprint. Discussion started: 5 August 2024

Atmospheric Measurement Techniques Discussions
Open Access
EGU

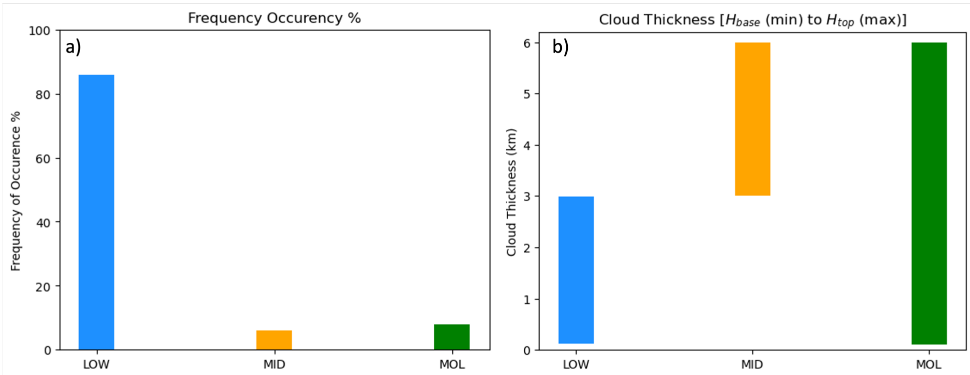

Figure 3. (a) The occurrence frequencies of single-layered LOW, MID, and MOL clouds, b) the average thickness for each cloud type.

Figure 4 visualizes the LWP frequencies for each cloud type averaged from the 15 research flights along with the constrained LWP frequency which shows the percentage occurrence of LWP above the threshold of 10 g/m^2 for each cloud type. Amongst the 15 flights, the maximum average LWP is observed for MOL clouds at around 370 g/m^2 followed by LOW at 208 g/m^2 and very low for MID clouds at around 65.8 g/m^2. The overall statistical results for the LOW, MID, and MOL classified cloud types are summarized in Table 3.

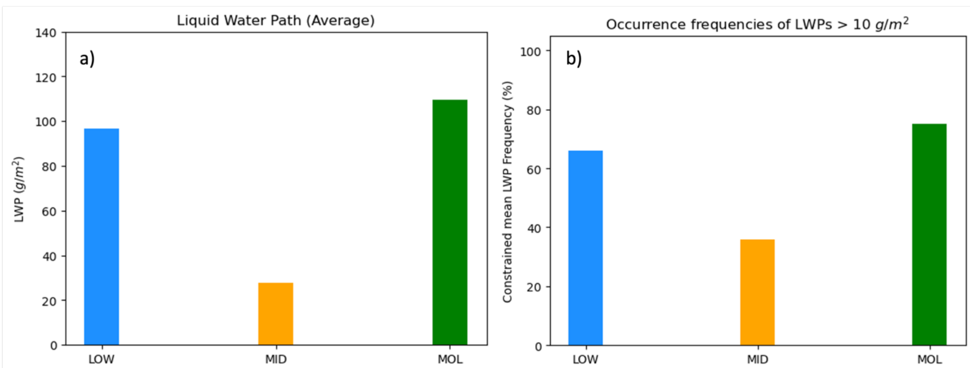

Figure 4. a) Averaged LWP for each cloud type from the 15 research flights. b) Constrained LWP occurrence frequencies for LWPs greater than 10 g/m^2 which is the threshold for classifying liquid and mix phase from ice-phase cloud transects. Percentages for LWP>10 g/m^2 are approximately 66%, 36% and 75% for LOW, MID and MOL clouds, respectively.

https://doi.org/10.5194/amt-2024-124
Preprint. Discussion started: 5 August 2024

Atmospheric Measurement Techniques
Discussions

Table 3. Mean, standard deviation, minimum and maximum ranges for the estimated cloud base and top heights along with the calculated LWP values for each single-layered cloud type.

	LOW	**MID**	**MOL**
H_{base} ± SD **Min, Max (km)**	1.01 ± 0.6 0.13, 2.97	4.16 ± 0.80 3.01, 5.97	1.56 ± 0.93 0.11, 2.99
H_{top} ± SD **Min, Max (km)**	1.57 ± 0.58 0.15, 2.99	4.79 ± 0.84 3.03, 5.99	4.18 ± 1.04 3.01, 5.99
LWP (mean) ± SD **Max (g/m^2)**	96.7 ± 187 2732	27.9±73 963	109.48 ± 208 2121

4 Low cloud phase retrieval results and discussions

As shown in Figure 3, LOW clouds are dominant cloud type (~90%) observed during SOCRATES. In this section, we discuss how to determine LOW cloud phase. The estimated cloud base and top heights, along with other radar-lidar and in-situ variables, were aggregated using the median to a temporal resolution of 10 seconds (0.1 Hz). This aggregation was constrained to the cloud boundaries and single-layered low-level cloud types to ensure a more continuous data distribution and to minimize outliers, thereby improving statistical consistency before phase determination.

4.1 Determination of Cloud Phase

Figure 5 describes the flow-chart of determining cloud phase for the classified low-level clouds (LOW) with cloud-top heights below 3 km after constraining for the in-cloud conditions (LWC>0.001 g/m^3). The phase partitioning method described in this section is used simultaneously as combined filters to classify the cloud phase as a 2-dimensional phase profile of liquid, mix and ice phase. LWP threshold was estimated after constructing probability density function (PDF) plots for the classified LOW, MID, MOL, HGH, and HOM clouds which returned a peak of less than 10 g/m^2 in LWP values for the HGH and HOM clouds which are prevalently ice-dominated clouds. There are significant overlaps between the LWP PDFs for classified cloud types, which results in some inconsistencies and uncertainties. For example, LOW clouds also display a peak in LWP values less than 10 g/m^2 but simultaneously also show consistently greater frequency for LWP values even greater than 200 g/m^2. Whereas the LWP frequencies for other cloud types diminish to zero after 15 or 20 g/m^2. The LWP value of ~10 g/m^2 also lies around the uncertainty value for LWP measurement over SO (Kang et al., 2021). While LWP values for LOW, MID and MOL cloud types are significantly higher, most of the LWPs for HGH and HOM clouds are below 10 g/m^2. Therefore, we use LWP=10 g/m^2 as a threshold to determine cloud phases where cloud samples with LWP < 10 g/m^2 is classified as ice clouds, while LWP >= 10 g/m^2 as mixed-phase or liquid clouds.

https://doi.org/10.5194/amt-2024-124
Preprint. Discussion started: 5 August 2024

Atmospheric Measurement Techniques
Open Access
Discussions

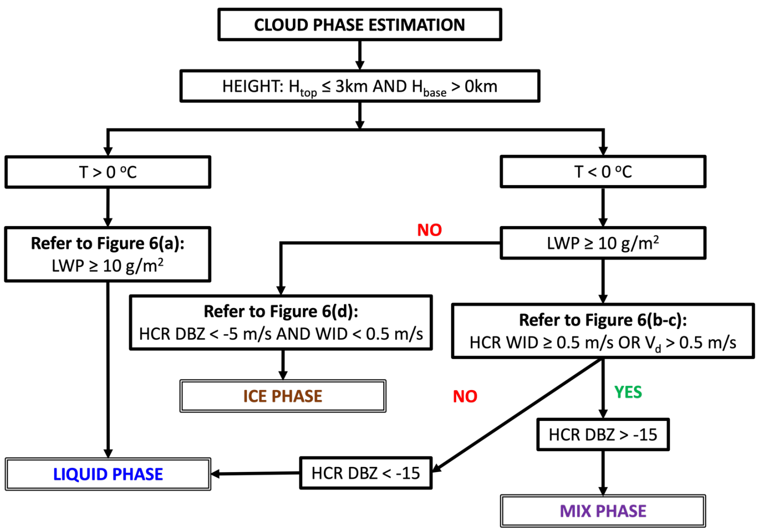

Figure 5. Flow chart depicting the phase classification of single-layered LOW clouds during SOCRATES. Spectrum Width (WID), Doppler Velocities (V_d) and reflectivity (dBZ) are measured by HCR radar, and Liquid Water Path (LWP) is calculated from in-situ measurements. Temperature is provided from ERA5 reanalysis air temperature product matched to the HCR-HSRL merged dataset.

In addition to the LWP threshold, the profile of atmospheric temperature provides another threshold for determining LOW cloud phase. where temperature is greater than 0 ºC is classified as liquid while for temperature between -40 to 0 ºC is further analyzed for categorizing between liquid, mixed and ice. As shown in Fig. 5, if LWPs are equal or greater than 10 g/m^2 and T is higher than 0 ºC, then the cloud samples are classified as liquid clouds. For ice clouds, it is as simple as classifying liquid clouds where the cloud samples are defined ice clouds when both LWP < 10 g/m^2 and T < 0 ºC, whereas it becomes more complicated for mixed-phase clouds. For the cloud samples with T > 0ºC and reflectivity < -15 dBZ are considered as liquid cloud droplets because most of drizzle drops have higher reflectivity (> -15 dBZ, Wu et al., 2020). Low WIDs correspond to homogenous single-phase of cloud hydrometeors while a broad range of WIDs suggest multiple phases and/or significant turbulence and wind shear (Shupe., 2007). The regions with both low WID and V_d (< 0.5 m/s, weak turbulence) are classified as liquid phase with dominant small liquid cloud droplets and SLW. The cloud samples are classified as mixed-phase clouds when both Doppler spectrum width (WID) and Doppler velocity (V_d) values are greater than 0.5 m/s (downdraft) which represent a greater variability of velocity, greater turbulence in cloud droplets and variable size distribution including large ice or drizzle-sized particles. The cloud samples with either WID > 0.5 m/s and V_d < 0.5 m/s (or WID < 0.5 m/s and V_d > 0.5 m/s) i.e. regions of high WID but low V_d (updrafts) or low WID and high V_d (downdrafts) are re-classified into mixed phase if the reflectivity (dBZ) > -15 and liquid phase if the reflectivity (dBZ) < -15. Radar reflectivity is a function of the sixth moment of the particle size (Wang et al., 2009) hence small and uniform liquid cloud droplets exhibit significantly lower reflectivity while mixed-phase clouds normally exhibit higher reflectivity values with a higher in-homogenous particle size distribution and greater density variability. Furthermore, the cloud samples with reflectivity > 5 dBZ represent precipitation (rain or snow depending on the temperature) and hence these samples are omitted in this study. Furthermore, the cloud samples with reflectivity > 5 dBZ represent precipitation (rain or snow depending on the temperature) and hence these samples are omitted in this study.

The estimation of WID, V_d, and dBZ thresholds was determined by the average values observed for each cloud layer based on the tropospheric height and at the estimated cloud base. These values were aggregated by prioritizing regions with more measurements over those with less ones, along with considering the cloud density at each layer, further comparing with existing studies, such as Xi et al. (2022) and Shupe (2007). Although these constraints were specifically tuned for clouds sampled during the SOCRATES campaign, we expect them to be broadly applicable to MBL clouds over the Southern Ocean.

To further demonstrate our phase classification methodology using T, LWP, WID, V_d, and the reflectivity (dBZ) as shown in Fig. 5, we present the bivariate histograms of liquid, mixed-phase and ice clouds in Fig. 6. Figure 6a illustrates the liquid cloud droplets, drizzle and rain drops based on radar reflectivity (-15 dBZ and 5 dBZ) and Doppler velocity (V_d<0.5 m/s) at higher temperatures (T>0 ºC). As shown in Fig. 6a, drizzle drops are dominant in the liquid clouds at T>0 ºC, with higher radar reflectivity and Doppler velocity. Marcovecchio et al., 2024 found that there is a higher drizzle frequency rate (71.8%) over SO using the ship-based radar-lidar measurements during the Measurement of Aerosols, Radiation, and CloUds over the Southern Ocean (MARCUS) field campaign than the ground-based radar-lidar measurements at the ARM East North Atlantic (ENA) site (45.1%). Figures 6b-6c present the classification of mixed-phase and liquid clouds where WID ≥ 0.5 or < 0.5 m/s, with T < 0 ºC and LWP ≥ 10 g/m2, using V_d and dBZ thresholds, where higher dBZ (>-15) corresponds to mixed while lower dBZ (<-15) and lower V_d (<0.5 m/s) corresponds to liquid phase. Liquid droplets due to their smaller size and uniform homogenous distribution exhibit lower dBZ, and lower V_d (updraft). Higher WID in liquid droplets mostly represent regions of turbulence and wind shear. The 2D pattern in Fig. 6c mimics that of Figure 6a, indicating that liquid clouds with more drizzle and mixed-phase clouds are dominant for LOW clouds over SO. There is a linear relationship between cloud reflectivity (dBZ) and Doppler velocity (V_d) for ice clouds, similar to liquid and mixed-phase clouds, except for Fig. 6b. Figure 6(d) represents regions classified as ice based on lower temperatures (T<0 ºC) and LWP < 10 g/m^2. The results of Figs. 6c and 6d suggest that the ice particle size distributions are not as broader as expected even though their particle sizes are much larger with higher radar reflectivity and Doppler velocity. The threshold of very high reflectivity, dBZ > 5 represents regions of precipitation (rain or snow) and is not considered in the final phase classification.

The phase classification methodology illustrated in Figs. 5 and 6(a-d) are used together simultaneously for estimating the liquid, mixed and ice phases for the low-level clouds in this study. The described method using radar-retrieved and in-situ measurements in this study was compared with the similar thresholding values defined in previous studies (Xi et al., 2022; Romatschke & Vivekanandan., 2023; Desai et al., 2023; Wu et al., 2020; Shupe., 2007) for coherence and consistency in the phase retrieval methodology. There could be some cases where the specified V_d and the WID threshold yield in a mix or liquid-phase conditions even if the true dominant phase is ice at that level (Shupe, 2007).

A 2-dimensional cloud phase is determined as a time-height dimensional profile for the valid cloud segments based on the discussed phase estimation method. Furthermore, the 2D phase profile is used to find a 1-dimensional dominant phase profile along the time dimension, where the dominant phase is determined by finding the sample that has the highest sample count along any vertical transect. For example, if at any time interval the sample count of a particular phase (say Liquid) is greater than the sample count of the other two phases (Ice and Mix) along the vertical transect, then liquid is the dominant phase at that time interval, i.e. the phase with the majority sample count at a vertical column is the dominant phase at that instance. Furthermore, if the sample count of ice is equal to liquid along any vertical transect, then the dominant phase at that time interval is mixed phase. This 1-dimensional dominant phase with a temporal resolution of 10 seconds phase partitioning will be used to determine the phase-specific cloud macrophysical results in the next section.

https://doi.org/10.5194/amt-2024-124
Preprint. Discussion started: 5 August 2024

Atmospheric Measurement Techniques Discussions

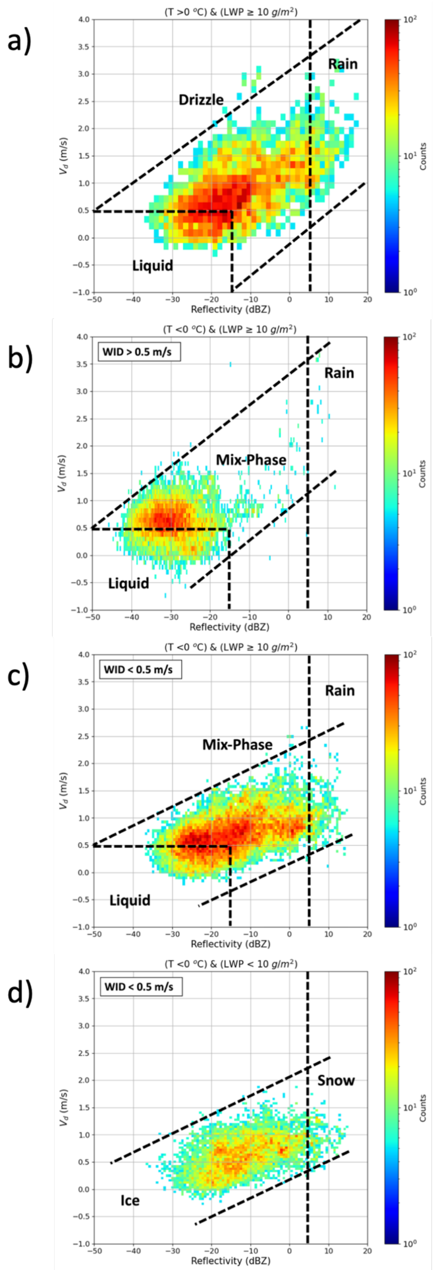

391
392 **Figure 6. (a-d) The bivariate histograms of radar reflectivity (dBZ) and Doppler velocity (V_d) for**
393 **different spectrum widths (WID), LWPs and Temperatures (T) to demonstrate the classified**
394 **liquid, ice and mixed phase cloud samples. The colorbar shows the sample count in each bin in a**
395 **logarithmic scale and the dashed lines represent the threshold values for the phase classification.**
396 **It is to be noted that the categories rain, drizzle, and snow are not taken into consideration in this**
397 **study.**

https://doi.org/10.5194/amt-2024-124
Preprint. Discussion started: 5 August 2024

Atmospheric Measurement Techniques
Discussions

4.2 Cloud Phase Determination Results

The liquid-phase clouds are firstly determined where both temperature (T) is greater than 0 ºC and cloud LWP is greater than 10 g/m^2, while when T is lower than 0 ºC and cloud LWP is greater than 10 g/m^2, the SLW clouds are determined when both WID and V_d are less than 0.5 m/s. Large ice particles are much heavier than small liquid cloud droplets with a broader spectrum width and greater fall speeds (Xi et al., 2022). The dependence on a linear LWP calculation as per the phase algorithm in this study adds some difficulty in resolving the exact hydrometeor phase in a vertical column. For instance, there could be cloud layers with an ice-phase top and liquid or mix-dominated base, but the LWP constraint considers the whole column to be ice-phase if the LWP < 10 g/m^2. A significant number of mixed-phase cloud samples were found at the cloud base due to broader WID and larger V_d values, which could be attributed to the presence of either larger drizzle drops or ice particles.

These estimated phase retrievals are illustrated in Fig. 7(a-h) from one selected case, which was chosen arbitrarily to offer visual clarity in phase profiles. The cloud phase presented in Fig. 7g is the 2-dimensional phase retrieval method but may be not highly depictive of the actual cloud phase, whereas Fig. 7h is the dominant cloud phase for each vertical transect retrieved from the 2D phase data where a phase is considered dominant if its sample count is greater than the other two in the same vertical column. This dominant cloud phase inferred from this 2D data along the vertical axis returns reasonably accurate findings compared to other phase detection studies over the SO. Note that the cloud phase is not available for very low LWC values due to the constraint used for in-cloud conditions.

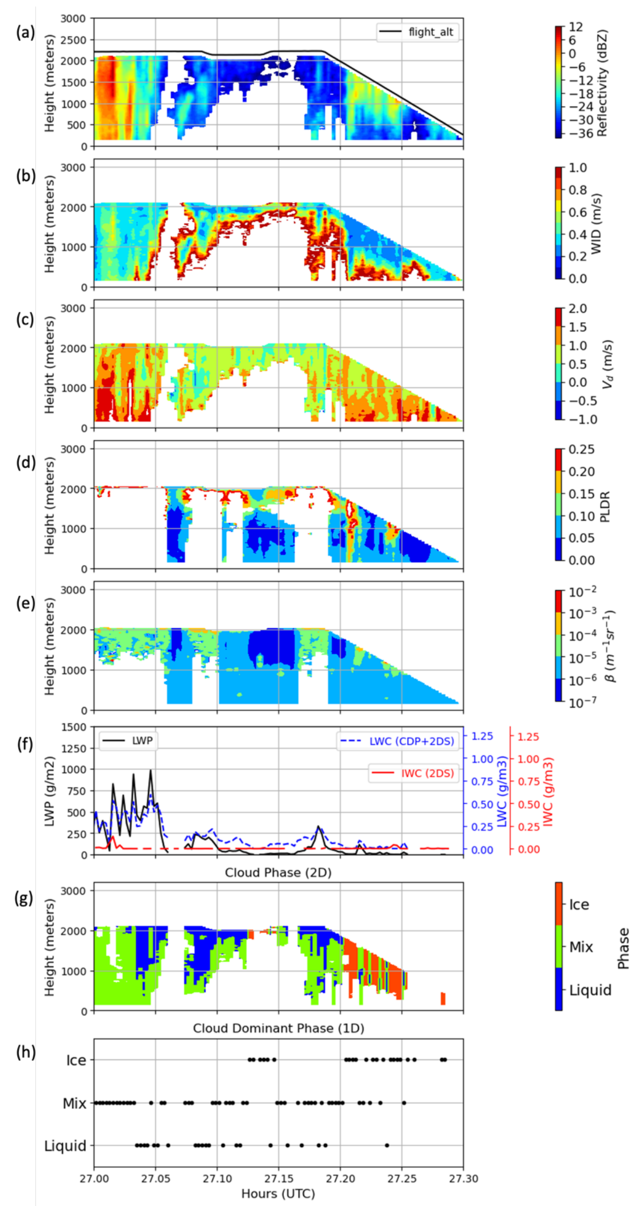

Figure 7. A case study for flight RF09 during SOCRATES illustrating the phase-detection algorithm in this study. (a) The HCR Reflectivity (dBZ) with the flight altitude in meters (black line), (b) Spectrum Width (WID), and (c) Doppler Velocity (V_d) profiles. (d) and (e) represent the HSRL (lidar) Particle Depolarization Ratio (PLDR) and Backscatter Coefficient (β). (f) represents the LWP, LWC, IWC values for each determined phase in (d). (g) and (h) represent the determined 2-D and dominant cloud phase. The time series is in decimal points where 27 hours is 3:00 UTC.

https://doi.org/10.5194/amt-2024-124
Preprint. Discussion started: 5 August 2024

Atmospheric Measurement Techniques Discussions

Higher IWC values correspond to ice phase particles greater than 200 µm in size. It is noticeable that the ice phase also exists for very low or negligible IWC values which correlates to very small-sized ice particles. The cloud transects where the dominant phase is liquid but also has a significant amount of mixed phase around the cloud base is mostly indicative of drizzle or precipitation-size particles.

Inspecting the 2DS particle probe imagery (not shown in this paper) reveals that liquid cloud droplets are mostly present in the form of spherical shape, and large ice particles have irregular shape, while small ice particles cannot be resolved very well using the 2DS probes. The 2DS images demonstrate that liquid cloud droplets are dominant at the upper levels of cloud layer, while a mixture of liquid cloud droplets and ice particles exists at the lower levels. Large ice particles (D_p > 50 µm) are easily identified by 2DS images, while it is challenging to distinguish small ice particles with cloud droplets from 2DS imagery. D'Alessandro et al. (2021) developed a phase-determination method by visually inspecting the 2DS particle imagery for particles of size greater than 50 µm and feeding this training data to a multinomial logistic regression (MLR) model to classify them as liquid, mix or ice phase. For the particles of size smaller than 50 µm, they were classified using a simple CDP number concentration thresholding method: $N_c < 1$ cm^{-3} corresponds to ice phase and $N_c > 1$ cm^{-3} represents liquid phase.

Table 4a lists the comparison of the phase determination using the MLR method (D'Alessandro et al., 2022; 2021) and this study. With a total of 2335 overlapping samples, there are 45.7%, 26.2% and 28.0% of classified liquid, mixed-phase and ice clouds from this study, while they are 80.4%, 11.6% and 7.9% from the MLR method. This comparison indicates that more liquid, but less mixed-phase and ice cloud are identified by the MLR method than our results for the overlapping samples. Of the three categories, there are a total of 995 samples of liquid clouds are identified by both the MLR method and our study at the same timestamps, which accounts for 93.3% of classified liquid clouds from this study and 53.0% of classified liquid clouds from the MLR method. The overlaps in ice and mixed-phase clouds from these two methods are much less than their liquid cloud counterparts. The 162 (140) overlapping samples for ice (mix) correspond to 87% (51%) of classified ice (mix) cloud samples from MLR method and 24.7% (22.83%) of classified ice (mix) samples detected by this study. Note that these percentages are just based on the matched dataset samples and do not represent the entire dataset for both MLR, and the dominant cloud phase determined by this study.

To further evaluate the cloud phase partitioning method, we compare the classified phases from this study with the MLR method and Shupe et al. (2005) and Intrieri et al. (2002) method for the classified low-level cloud samples for the 15 research flights during SOCRATES. Shupe et al. (2005) and Intrieri et al. (2002) used the lidar median PLDR (particle depolarization ratio) values to classify liquid (PLDR < 0.11), mix (0.11 < PLDR <0.15) and ice (PLDR>0.15), respectively. As expected, the percentages determined by this study in Table 4b are similar to the results in Table 4a, the percentage of liquid clouds classified by this study is ~10 to 20% lower, but ~10 to 15% higher in mixed-phased clouds compared to those classified from both the methods of MLR and Shupe et al. (2005). The ice clouds classified from this study are ~15% higher than those detected by MLR but ~10% lower than those classified using Shupe. (2005) and Intrieri. (2002) method. This comparison is very reasonable given that our method is developed from aircraft in measurements and radar-measurements over SO, while the method developed by Intrieri et al., 2002 and Shupe et al., 2005 were based on the ground-based lidar measurements over Arctic regions and MLR uses a machine learning algorithm trained over the in-situ cloud and drizzle droplet measurements (CDP+2DS). The other reason for the difference lies in the in-cloud constraints (LWC>0.001 g/m^3 to define in-cloud samples) used in our method which were not used for the other two methods. Furthermore, MLR also reported a significantly high number of unclassified cloud samples (~56%) for aircraft-measured in-situ temperatures above freezing point (>0°C) which were not included in this phase-percentage calculation for low clouds using MLR (Table 4(b) column 2).

https://doi.org/10.5194/amt-2024-124
Preprint. Discussion started: 5 August 2024

Atmospheric Measurement Techniques
Discussions

If we treat the results classified in this study as a reference, the lidar median PLDR values to classify liquid, mixed and ice clouds may need to be tuned slightly for SO low clouds. The existing PLDR thresholds (<0.11 for liquid, 0.11-0.15 for mixed, and >0.15 for ice phase clouds) as defined by Sassen (1991), Intrieri (2002), and Shupe (2007), were originally established for Arctic clouds, which are characteristically different from the MBL clouds over the Southern Ocean (SO). Using the classified results in this study as a reference, we tune the existing HSRL PLDR thresholds for SO low-level clouds and have the updated thresholds of PLDR < 0.09 for liquid phase, 0.09-0.18 for mixed phase, and >0.18 for ice phase clouds. This adjustment was based on a simple analysis of the low cloud samples measured simultaneously by both radar and lidar. Further scrutiny may be necessary to estimate the accuracy of these thresholds for low-level clouds over SO, and this could be a focus for future research.

Table (4a). Comparison of the phase determination between MLR method cloud phase product (D'Alessandro et al., 2022) and this study matched at the same temporal resolution (10 secs). Presented number are raw sample counts.

MLR Method/ This Study	Ice (this study)	Mix Phase (this study)	Liquid (this study)
Ice (MLR)	**162**	16	8
Mixed Phase (MLR)	67	**140**	64
Liquid (MLR)	426	457	**995**

Table (4b). The cloud phase partitioning for each phase-type determined using this method (dominant phase) compared with the MLR method and Shupe (2005), Intrieri (2002) method for the classified low cloud samples during SOCRATES. The data is aggregated to a 10 second sample interval. The unclassified cloud samples in the MLR cloud phase product are not included in the sample % calculation in column 2, and the in-cloud constraint (LWC>0.001 g/m^3) is not included for phase detected by MLR (column 2) and Shupe (2005), Intrieri (2002) (column 3).

	This Study	MLR Method	Shupe et al., 2005; Intrieri et al., 2002 Method
Liquid %	45.4	71.7	52.3
Mix %	22.2	10.3	5.5
Ice %	32.5	18.0	42.2

As previously mentioned, it's important to note that these three classification methods are different. The MLR method determines cloud phase based on tuning a MLR (multinomial logistic regression) model to cloud hydrometeors sampled using the in-situ probes (CDP+2DS) onboard the NCAR/GV aircraft during SOCRATES, while we used both in-situ and radar measurements in this study. The HSRL lidar method is purely dependent on the PLDR thresholds. The HSRL lidar detects a smaller fraction of the cloud fraction compared to the HCR radar, as lidar is highly attenuated for thicker cloud layers whereas HCR radar can offer a well-resolved cloud profile. Consequently, the radar and lidar do not provide measurements for the exact same cloud layers, with an overlap region of only about 8%. Therefore, while the comparison between these three methods is not entirely straightforward, it provides a reasonable rough estimation for comparing the phase estimations across a linear time dimension.

https://doi.org/10.5194/amt-2024-124
Preprint. Discussion started: 5 August 2024

4.3 Cloud characteristics for each determined cloud phase

Table 5 lists the summarized macrophysical cloud properties for each classified phase, based on the 1-dimensional dominant phase from all 15 research flights during SOCRATES. The statistical results listed in Table 5 include sample counts (and percentages) along with mean and standard deviation for cloud-base and -top temperatures (T_{base} and T_{top}) and heights (H_{base} and H_{top}), cloud thickness (ΔH) and LWP.

Table 5. Summaries of cloud macrophysical properties for each determined cloud phase

Phase	Samples	T_{base} (°C)	T_{top} (°C)	H_{base} (km)	H_{top} (km)	ΔH (km)	LWP (g/m^2)
Ice	1043 (~32.5%)	-3.5±4.6	-6.0±4.8	1.12±0.63	1.59±0.61	0.47	2.7±2.6
Mixed-phase	712 (~22.2%)	-2.1±4.3	-8.2±4.8	0.74±0.53	1.65±0.60	0.91	200.5±267
Liquid	1458 (~45.4%)	-1.2±4.9	-3.9±5.4	0.90±0.54	1.34±0.59	0.44	89.7±100

4.3.1 Cloud-base and -top temperatures (T_{base} and T_{top})

Low clouds generally exhibit higher temperature trends than the recorded aircraft temperature at the actual flying levels because of the difference in tropospheric altitude of the flight and the actual cloud boundaries. The ERA5 air temperature is used to extract the temperature at the cloud base and cloud height altitudes. Figure 8(a) shows the occurrence probabilities of the estimated cloud phases against the ERA5 air temperature for the entire cloud transect, highlighting that all the cloud phases have the highest occurrence in the range of -5 to -2.5 °C, while no ice and mixed phase exist at temperatures greater than 0 °C, 100% liquid-phase concentration is observed at T >0 °C. The frequency distributions in Fig. 8 (b-c) show that all T_{top} samples from three phases increase monotonically from -20 °C, peak at -7.5 and -5 °C for mix and ice respectively, and -2.5 °C for liquid-phase, and quickly vanish after 0 °C except for liquid samples. The frequency distributions of T_{base} samples from three phases almost mimic their T_{top} counterparts but with different peaks: The maximum frequency of liquid and ice phase occurs at -2.5 °C, while mixed-phase T_{base} remains at 0 °C. The different peaks in T_{base} samples from three phases have reflected in their mean H_{base} where the mean ice-phase H_{base} is 1.12 km, higher than other two H_{base} (0.74 and 0.90 km). T_{base} and T_{top} for liquid phase have the highest frequency at near -1 °C. Ice and mixed-phase cloud temperatures show similar trends with most samples around lower temperatures. Interestingly the peaked T_{base} of mixed-phase clouds occurs at 0 °C because most of the mixed phase cloud samples occur around the cloud base where their temperatures are higher than cloud-top ones. It should also be noted that this analysis considers only the dominant phase for each layer (Fig. 8b-c), but the 2-dimensional phase is exclusively liquid for temperatures greater than 0 °C (Fig. 8a) as discussed in the phase determination method.

https://doi.org/10.5194/amt-2024-124
Preprint. Discussion started: 5 August 2024

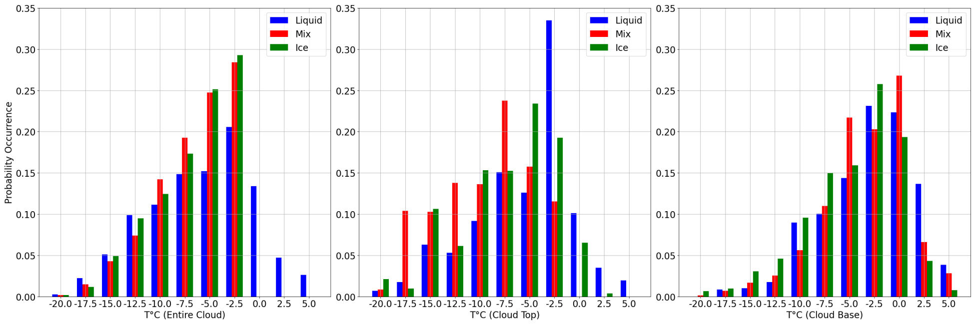

Figure 8. Probability distribution of the entire cloud layer temperature (T) from ERA5 air temperature, cloud-top (T_{top}) and cloud-base (T_{base}) temperatures for each determined phase

4.3.2 Profiles of determined cloud phase and radar observations

Figure 9 shows the vertical distributions of classified liquid, mixed-phase and ice cloud samples, as well as the total samples of LOW clouds from 0 to 3 km (retrieved from the 2-dimensional cloud phase profile). As mentioned above, liquid clouds are dominant, and its occurrence has the highest frequency around 0.75 – 1.2 km. The ice cloud occurrence follows the trend of liquid clouds with the higher frequencies at the levels of 0.75-1.5 km. Differing to liquid and ice clouds, the mixed-phase occurrence is evenly distributed in the cloud layer with higher sample counts from 0.5 km to 1.5 km. It should be noted that the sample counts of all three phases diminish to 0 at around 150 m which is where the estimated cloud base lies for low clouds in this study.

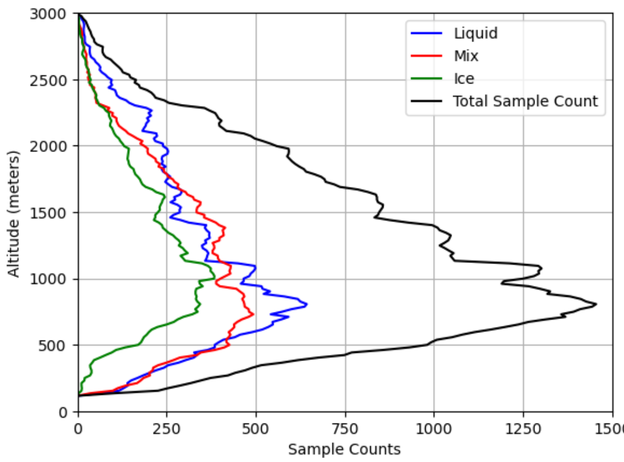

Figure 9. Profiles of the cloud samples for each determined cloud phase along with the total sample number (black line).

To further investigate the vertical distribution of classified liquid, mixed-phase, and ice clouds in LOW clouds during SOCRATES, we plot the normalized vertical distributions of HCR reflectivity (dBZ), Doppler Velocity (m/s) and Spectrum Width (m/s) in Fig. 10 (Contoured Frequency Altitude Diagram, CFAD).

Figures 10a-10c show the CFADs of determined liquid cloud samples where most of radar reflectivity dBZ values range from -35 to -25 with the median values of ~-25 dBZ, except for lower bottom regions of the cloud (normalized height, H_i < 0.2).. The nearly constant median values with height, and moderate dBZ, V_d and WID, indicate the liquid cloud microphysical properties vary slightly within cloud layer with a moderate range of cloud droplets. The maximum occurrences of V_d and WID for liquid clouds are ~ 0.0 m/s and 0.2 m/s. Much higher V_d and WID at the low bottom regions indicate that there are some large drizzle drops with a broader size distribution, however the number concentrations of these large drizzle drops are not higher enough to significantly contribute radar reflectivity. Based on the aircraft in situ measurements during SOCRATES (Zheng et al. 2024), the cloud droplet and drizzle radii near cloud base are one order of magnitude difference (7 µm vs. 70 µm), whereas their number concentrations are four orders of magnitude difference (100 cm^{-3} vs. 10^{-1} cm^{-3}). These lower number concentrations may attribute to the lower reflectivity near cloud base in Fig. 10a. Another possible reason to explain the contradicted relationship between radar reflectivity and V_d/WID is not enough liquid samples at the lower bottom regions, which can't be ruled out.

Compared to the CFADs of liquid cloud samples, the mixed-phase clouds have a broader and higher radar reflectivity dBZ values with the maximum frequencies occur at ~ -10 dBZ around mid-cloud layer, presumably due to their larger particle size and irregular shape or morphology. Correspondingly, their median values are also much large (-15 ~ -10 dBZ), except for the lower bottom regions (H_i < 0.2). The CFADs of V_d for mixed-phase clouds mimic the shape of liquid cloud samples but with higher maximum occurrence at ~0.5 m/s and their median values increase monotonically from cloud top (~ 0.6 m/s) to cloud base (~1.3 m/s), indicating that cloud droplets or ice particles increase from cloud top to cloud base, much faster at the lower bottom regions. Consequently, there are more large drizzle drops or ice particles near cloud base with significant downwelling movement and the prevalence of a broader size distribution of particles. Surprisingly, the CFADs of WID for mixed-phase clouds are similar to those of liquid clouds, but not as broader as liquid clouds at the lower bottom regions. These results suggest that the well-mixed cloud droplets/drizzles and ice particles at the lower bottom regions make particle size broader and larger WID values, but they are not as broader and higher WID as liquid clouds where more both cloud droplets and drizzle drops co-exist near cloud base.

For ice clouds, their CFADs of V_d are similar to those of liquid clouds, however, their CFADs of radar reflectivity and WID significantly differ to those of liquid and mixed-phase clouds. Most of radar reflectivity dBZ values range from -45 to -25 at the upper regions of cloud layer with the median values of ~-30 dBZ. Surprisingly, these ice particles with lower radar dBZ values have a much higher WID value, up to 0.8 m/s, and lower V_d values (~ 0-0.2 m/s). These results indicate that most ice particles for SO low clouds have small particles but with a broader size distribution. The CFADs of ice clouds at the upper regions of cloud layer are consistent to those CFADs of liquid and mixed-phase clouds at the lower bottom regions, suggesting that the lower dBZ regions where small cloud droplets or ice particles are dominant can have a broader size distribution for SO low clouds.

https://doi.org/10.5194/amt-2024-124
Preprint. Discussion started: 5 August 2024

Atmospheric Measurement Techniques
Open Access
EGU
Discussions

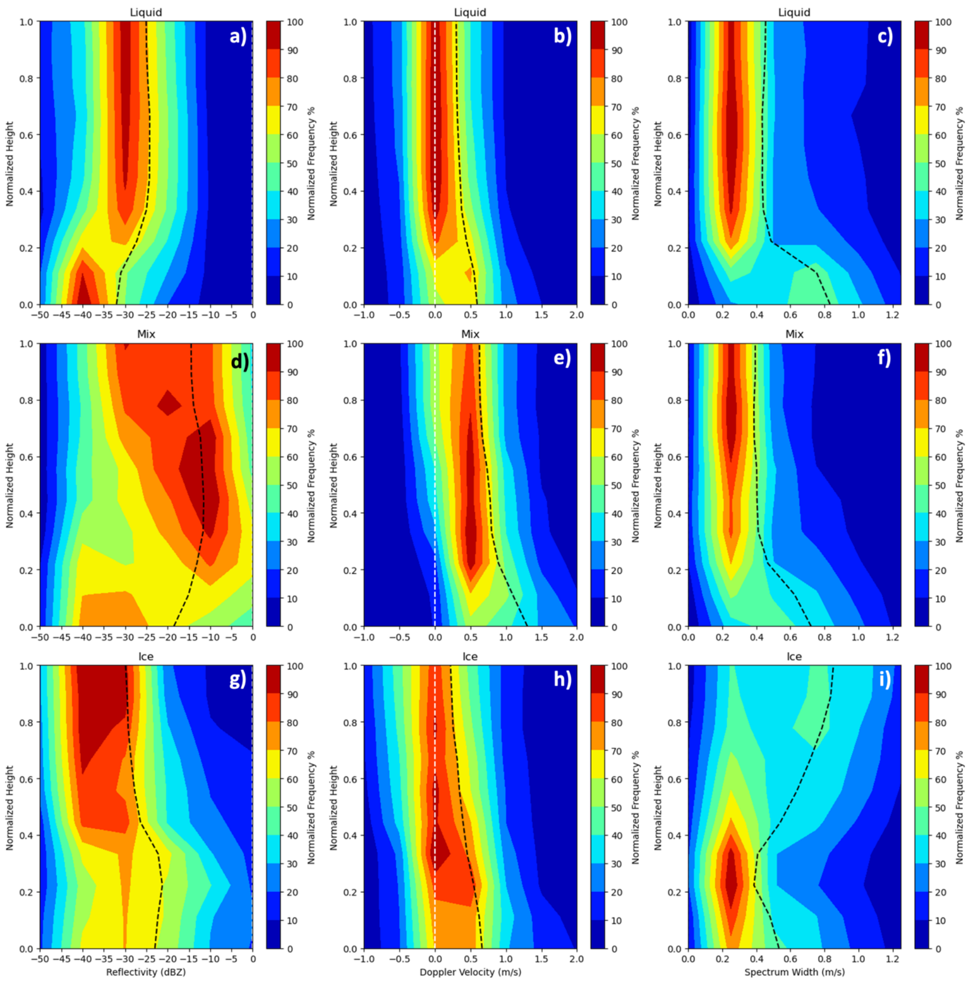

Figure 10. Normalized vertical distributions of radar reflectivity (dBZ), Doppler velocity V_d (m/s) and spectrum width (m/s) for the classified liquid (a-b), mixed (d-f), and ice (g-i) clouds. during SOCRATES. Height normalization is determined by $H_i = \frac{H - H_{base}}{H_{top} - H_{base}}$, where the cloud top is denoted as 1 and base as 0. The median values are represented using the black dashed lines and the white lines in V_d denote 0 m/s. The colorbar denotes the occurrence frequency (%).

V_d and WID are codependent variables as V_d indicates the motion of the hydrometeor samples moving away or towards the radar, however WID is indicative of the spread or variability in the velocity distribution. For an example, a positive (negative) V_d represent a downdraft (updraft) motion, but a high (low) WID indicates a significant variability in the velocities, including greater (lower) turbulence and wind shear, which can be interpreted as a broader (narrower) size distribution. The regions with high WID but low V_d can be explained as that the average velocity of the cloud particles within the radar's sampling volume is low, but with a significant spread or variability in their individual velocities due to significant turbulence, wind shear, or different particles sizes. Conversely, a high V_d but a small WID suggests the either large drizzle drops, or ice particles are moving (downward) rapidly but uniformly with a narrow size distribution.

https://doi.org/10.5194/amt-2024-124
Preprint. Discussion started: 5 August 2024

The CFAD plots in Fig. 10(a-i) display noticeable skewness. Generally, the frequency plots are skewed to the right, but in Fig. 10(d), the dBZ frequency for mixed-phase samples is skewed to the left due to the higher reflectivity values observed for mixed-phase clouds. Moreover, the median values (black dashed lines in Fig. 10) are significantly shifted towards higher values of WID and Vd near the cloud base, while they shift towards lower values in dBZ for liquid and mixed phase clouds in Fig. 10(a and d). This phenomenon can be attributed to the majority of cloud droplets exhibiting lower reflectivity yet significantly higher values for spectrum width and Doppler velocity at the estimated cloud base. Contributing factors include lower sample counts, and increased turbulence or wind shear contributing to evaporation of particles around the estimated cloud base. Additionally, this observation also results from the nature of cloud sampling during SOCRATES as demonstrated in Fig. 7(a-c), which introduces greater volatility in recorded datasets due to the proximity of the aircraft to the cloud layers compared to ground-based or satellite remote sensing.

5 Summary and Conclusions

This study developed a phase detection method using HCR radar and in-situ measurements to determine the cloud phase over the Southern Ocean for low-level clouds sampled during the 15 research flights of the SOCRATES campaign. The macrophysical properties and statistical results for the different types of clouds and their correspondingly classified phases were discussed. Finally, the vertical distribution for each phase-specific radar retrieved parameters was presented. Comparisons of this study with existing literature were also discussed. The following conclusions were finally drawn:

1. A new method based on radar reflectivity and spectrum width gradient was developed to estimate cloud boundaries and classify cloud types as LOW, MID, and MOL based on the estimated cloud-top and -base heights. LOW-type clouds with H_{base} and H_{top} below 3km were found to be the most prevalent with almost 90% occurrence frequency. Liquid Water Path was calculated for each cloud type using the estimated cloud heights and a merged CDP+2DS LWC measurement, with an uncertainty of around 10 g/m^2. Average LWP values for LOW, MOL and MID clouds are 96.7 g/m^2, 109.48 g/m^{2,} and 27.9 g/m^2, respectively.
2. A phase determination method was developed to classify the single-layered low-level (LOW) clouds as liquid, mixed, and ice phases with the occurrence frequencies of 45.4%, 22.2% and 32.5%, respectively. Comparison with the MLR phase detection method by D'Alessandro et al. (2021), and Shupe et al. (2005) and Intrieri et al. (2002) method which used lidar PLDR thresholds, showed that the percentage of liquid clouds classified by this study is ~10 to 20% lower, but ~10 to 15% higher in mixed-phased than the results from other two methods, while the classified ice clouds from this study are ~15% higher than those detected by MLR but ~10% lower than those classified using Shupe. This comparison is quite reasonable, as our method is derived from aircraft measurements and radar observations over SO while the methods developed by Intrieri et al. (2002) and Shupe et al. (2005) were based on ground-based lidar measurements in Arctic regions. Additionally, the MLR method employs a machine learning algorithm trained on in-situ cloud and drizzle droplet measurements (CDP+2DS). Using the classified results in this study as a reference, we tune the existing HSRL PLDR thresholds for SO low-level clouds and have the updated thresholds of PLDR < 0.09 for liquid phase, 0.09-0.18 for mixed phase, and >0.18 for ice phase clouds.
3. For the low-level clouds from 0 to 3 km, the mixed-phase cloud dominates near cloud base (<1 km) but are well distributed along the vertical cloud layer which could be attributed to large drizzle drops or ice particles. The ice-phase clouds are prevalent from the mid to top cloud level (1-3km), while most of the liquid-phase clouds are located in the lower mid-cloud range (from 500 m to 1 km).

4. The normalized vertical profiles (CFADs) of radar reflectivity, Doppler velocity (Vd) and spectrum (WID) for each determined cloud phase show that the liquid and ice clouds have the lowest reflectivity values, with median reflectivities of around -30 to -25 dBZ, while mixed-phase clouds have a higher median reflectivity of around -15 to -10 dBZ due to large drizzle drops or ice particles. Higher Doppler velocity and Spectrum Width at the cloud base indicate greater drizzle or particle concentrations with significant downwelling movement and the prevalence of a wider size distribution of particles. The CFADs of ice clouds at the upper regions of cloud layer, lower dBZ values but larger WID values, are consistent to the CFADs of liquid and mixed-phase clouds at the lower bottom regions. These results indicate that small cloud droplets or ice particles (lower dBZ) for SO LOW clouds can have a broader size distribution (large WID).

In conclusion, the results presented in this study provide comprehensive statistical and phase-relevant macrophysical properties for the low-level clouds sampled during the SOCRATES campaign, along with presenting new methods to estimate cloud boundaries and determine the dominant cloud phase. These results would improve the current understanding of the low-level Southern Ocean cloud properties and further aid in improving model simulations and better representation of the climate.

Data Availability. All the data and the relevant instrumentation details (radar-lidar and in-situ) for the NSF SOCRATES campaign used in this study are freely accessible from the EOL data archive https://data.eol.ucar.edu/dataset/ and the official website https://www.eol.ucar.edu/field_projects/socrates. The MLR cloud phase product dataset is available at https://doi.org/10.26023/S6WS-G5QE-H113.

Author contributions. The idea of this study was discussed by AD, BX, and XD. AD performed the analyses and wrote the paper. AD, BX, XD, and XZ participated in the scientific discussions and provided substantial comments and edits on the paper.

Competing interests. The contact author has declared that neither they nor their co-authors have any competing interests.

Acknowledgments. The aircraft measured dataset and the SOCRATES campaign relevant details along with the list of publications are available free to access at https://www.eol.ucar.edu/field_projects/socrates. Special thanks to John D'Alessandro (University of Washington) for helping understand the working of the MLR method for phase determination, Ulrike Romatschke (NCAR) for explaining the radar-lidar constrained fuzzy logic parameters for the cloud and drizzle hydrometeor types, and Christopher J. Webster (NCAR) for helping to troubleshoot and run the XPMS2D software to visualize the 2DS probe imagery. The draft of this paper was briefly proofread using the AI tools Grammarly and ChatGPT for final revisions.

Financial Support. This work was supported by the University of Arizona's IT4IR TRIF and Provost Investigation funds. The researchers at the University of Arizona were also supported by NSF grant AGS-2031750 at the University of Arizona.

References

Atlas, R., Mohrmann, J., Finlon, J., Lu, J., Hsiao, I., Wood, R., & Diao, M.: The University of Washington Ice-Liquid Discriminator (UWILD) improves single-particle phase classifications of hydrometeors within Southern Ocean clouds using machine learning, Atmospheric Measurement Techniques, 14(11), 7079–7101, https://doi.org/10.5194/amt-14-7079-2021, 2021.

https://doi.org/10.5194/amt-2024-124
Preprint. Discussion started: 5 August 2024

Baker, B., Mo, Q., Lawson, R. P., O'Connor, D., & Korolev, A.: Drop Size Distributions and the Lack of Small Drops in RICO Rain Shafts, J. Appl. Meteor. Climatol., 48, 616–623, https://doi.org/10.1175/2008JAMC1934.1, 2009.

Bodas-Salcedo, A., Hill, P. G., Furtado, K., Williams, K. D., Field, P. R., Manners, J. C., et al.: Large contribution of supercooled liquid clouds to the solar radiation budget of the Southern Ocean, Journal of Climate, 29(11), 4213–4228, https://doi.org/10.1175/JCLI-D-15-0564.1, 2016.

Cesana, G., & Chepfer, H.: Evaluation of the cloud thermodynamic phase in a climate model using CALIPSO-GOCCP, Journal of Geophysical Research: Atmospheres, 118(14), 7922–7937, https://doi.org/10.1002/jgrd.50376, 2013.

D'Alessandro, J. J., Diao, M., Wu, C., Liu, X., Jensen, J. B., & Stephens, B. B.: Cloud phase and relative humidity distributions over the Southern Ocean in austral summer based on in situ observations and CAM5 simulations, Journal of Climate, 32(10), 2781–2805, https://doi.org/10.1175/JCLI-D-18-0232.1, 2019.

D'Alessandro, J. J., McFarquhar, G. M., Wu, W., Stith, J. L., Jensen, J. B., & Rauber, R. M.: Characterizing the Occurrence and Spatial Heterogeneity of Liquid, Ice, and Mixed Phase Low-Level Clouds Over the Southern Ocean Using in Situ Observations Acquired During SOCRATES, Journal of Geophysical Research: Atmospheres, 126(11), https://doi.org/10.1029/2020JD034482, 2021.

D'Alessandro, J., Schima, J., McFarquhar, G.: SOCRATES Cloud Phase Product. Version 1.0. UCAR/NCAR - Earth Observing Laboratory [data set], https://doi.org/10.26023/S6WS-G5QE-H113, 2022.

Desai, N., Diao, M., Shi, Y., Liu, X., & Silber, I.: Ship-Based Observations and Climate Model Simulations of Cloud Phase Over the Southern Ocean, Journal of Geophysical Research: Atmospheres, 128(11), https://doi.org/10.1029/2023jd038581, 2023.

Dong, X., Xi, B., Kennedy, A., Minnis, P., & Wood, R.: A 19-Month Record of Marine Aerosol–Cloud–Radiation Properties Derived from DOE ARM Mobile Facility Deployment at the Azores. Part I: Cloud Fraction and Single-Layered MBL Cloud Properties, J. Climate, 27, 3665–3682, https://doi.org/10.1175/JCLI-D-13-00553.1, 2014.

Eloranta, E. E.: High Spectral Resolution Lidar, In C. Weitkamp (Ed.), Lidar: Range-Resolved Optical Remote Sensing of the Atmosphere (pp. 143–163), Springer, https://doi.org/10.1007/0-387-25101-4_5, 2005.

Esselborn, M., Wirth, M., Fix, A., Tesche, M., & Ehret, G.: Airborne high spectral resolution lidar for measuring aerosol extinction and backscatter coefficients, Applied Optics, 47(3), 346–358, https://doi.org/10.1364/AO.47.000346, 2008.

Ewald, F., Groß, S., Wirth, M., Delanoë, J., Fox, S., & Mayer, B.: Why we need radar, lidar, and solar radiance observations to constrain ice cloud microphysics, Atmospheric Measurement Techniques, 14(7), 5029–5047, https://doi.org/10.5194/amt-14-5029-2021, 2021.

Hamilton, D. S., Lee, L. A., Pringle, K. J., Reddington, C. L., Spracklen, D. V., & Carslaw, K. S.: Occurrence of pristine aerosol environments on a polluted planet, Proceedings of the National Academy of Sciences, 111(52), 18466-18471, https://doi.org/10.1073/pnas.1415440111, 2014.

Hu, Y., Rodier, S., Xu, K., Sun, W., Huang, J., Lin, B., Zhai, P., & Josset, D.: Occurrence, liquid water content, and fraction of supercooled water clouds from combined CALIOP/IIR/MODIS measurements, Journal of Geophysical Research: Atmospheres, 115(D4), https://doi.org/10.1029/2010JD014002, 2010.

Humphries, R. S., Keywood, M. D., Gribben, S., McRobert, I. M., Ward, J. P., Selleck, P., Taylor, S., Harnwell, J., Flynn, C., Kulkarni, G. R., et al.: Southern Ocean latitudinal gradients of cloud condensation nuclei, Atmospheric Chemistry and Physics, 21(16), 12757-12782, https://doi.org/10.5194/acp-21-12757-2021, 2021.

Intrieri, J. M., Shupe, M. D., Uttal, T., & McCarty, B. J.: An annual cycle of Arctic cloud characteristics observed by radar and lidar at SHEBA, Journal of Geophysical Research: Oceans, 107(C10), SHE-5, https://doi.org/10.1029/2000JC000423, 2002.

Kang, L., Marchand, R., & Smith, W.: Evaluation of MODIS and Himawari-8 low clouds retrievals over the Southern Ocean with in situ measurements from the SOCRATES campaign, Earth and Space Science, 8(3), e2020EA001397, https://doi.org/10.1029/2020EA001397, 2021.

Kang, L., Marchand, R. T., & Wood, R.: Stratocumulus precipitation properties over the Southern Ocean observed from aircraft during the SOCRATES campaign, Journal of Geophysical Research: Atmospheres, 129(6), e2023JD039831, https://doi.org/10.1029/2023JD039831, 2024.

Kay, J. E., Hillman, B. R., Klein, S. A., Zhang, Y., Medeiros, B., Pincus, R., et al.: Exposing global cloud biases in the community atmosphere model (CAM) using satellite observations and their corresponding instrument simulators, Journal of Climate, 25(15), 5190–5207, https://doi.org/10.1175/JCLI-D-11-00469.1, 2012.

Kay, J. E., Wall, C., Yettella, V., Medeiros, B., Hannay, C., Caldwell, P., & Bitz, C.: Global climate impacts of fixing the Southern Ocean shortwave radiation bias in the Community Earth System Model (CESM), Journal of Climate, 29(12), 4617–4636, https://doi.org/10.1175/JCLI-D-15-0358.1, 2016.

Klein, S. A., Hall, A., Norris, J. R., & Pincus, R.: Low-cloud feedbacks from cloud-controlling factors: A review, Shallow clouds, water vapor, circulation, and climate sensitivity, Springer, 135–157, 2018.

Korolev, A., & Milbrandt, J.: How are mixed-phase clouds mixed?, Geophysical Research Letters, 49(18), e2022GL099578, https://doi.org/10.1029/2022GL099578, 2022.

Lance, S., et al.: Water droplet calibration of the Cloud Droplet Probe (CDP) and in-flight performance in liquid, ice and mixed-phase clouds during ARCPAC, Atmos. Meas. Tech., 3, 1683-1706, https://doi.org/10.5194/amt-3-1683-2010, 2010.

Lawson, R. P., O'Connor, D., Zmarzly, P., Weaver, K., Baker, B., Mo, Q., & Jonsson, H.: The 2D-S (stereo) probe: Design and preliminary tests of a new airborne, high-speed, high-resolution particle imaging probe, Journal of Atmospheric and Oceanic Technology, 23(11), 1462–1477, https://doi.org/10.1175/JTECH1929.1, 2006.

Lawson, R. P., Pilson, B., Baker, B., Mo, Q., Jensen, E., Pfister, L., & Bui, P.: Aircraft measurements of microphysical properties of subvisible cirrus in the tropical tropopause layer, Atmospheric Chemistry and Physics, 8(6), 1609–1620, https://doi.org/10.5194/acp-8-1609-2008, 2008.

Mace, G. G., Protat, A., Humphries, R. S., Alexander, S. P., McRobert, I. M., Ward, J., Selleck, P., Keywood, M., & McFarquhar, G. M.: Southern Ocean cloud properties derived from CAPRICORN and MARCUS data, Journal of Geophysical Research: Atmospheres, 126(4), e2020JD033368, https://doi.org/10.1029/2020JD033368, 2021.

https://doi.org/10.5194/amt-2024-124
Preprint. Discussion started: 5 August 2024

Atmospheric Measurement Techniques Discussions
Open Access
EGU

Marcovecchio, A. R., Xi, B., Zheng, X., Wu, P., Dong, X., & Behrangi, A.: What Are the Similarities and Differences in Marine Boundary Layer Cloud and Drizzle Microphysical Properties During the ACE-ENA and MARCUS Field Campaigns?, Journal of Geophysical Research: Atmospheres, 128(18), e2022JD037109, https://doi.org/10.1029/2022JD037109, 2023.

McCoy, D. T., Hartmann, D. L., & Grosvenor, D. P.: Observed Southern Ocean cloud properties and shortwave reflection. Part II: Phase changes and low cloud feedback, Journal of Climate, 27(23), 8858–8868, https://doi.org/10.1175/JCLI-D-14-00288.1, 2014.

McCoy, D. T., Burrows, S. M., Wood, R., Grosvenor, D. P., Elliott, S. M., Ma, P.-L., Rasch, P. J., & Hartmann, D. L.: Natural aerosols explain seasonal and spatial patterns of Southern Ocean cloud albedo, Science Advances, 1(6), e1500157, https://doi.org/10.1126/sciadv.1500157, 2015.

McFarquhar, G.: Measurements of Aerosols, Radiation, and Clouds over the Southern Oceans (MARCUS) Science Plan, United States, https://doi.org/10.2172/1253914, 2016.

McFarquhar, G. M., Finlon, J. A., Stechman, D. M., Wu, W., Jackson, R. M., & Freer, M.: University of Illinois/Oklahoma Optical Array Probe (OAP) Processing Software. Version 3.1.4, Zenodo [code], https://doi.org/10.5281/zenodo.1285969, 2018.

McFarquhar, G. M., Bretherton, C., Marchand, R. T., DeMott, P. J., Alexander, S. P., Protat, A., Roberts, G., Twohy, C. H., Toohey, D. W., Siems, S., et al.: New Unique Observations of Clouds, Aerosols and Precipitation over the Southern Ocean: An Overview of SOCRATES and MARCUS, in: Proceedings of the 15th Conference on Cloud Physics/15th Conference on Atmospheric Radiation, AMS, 2018.

McFarquhar, G. M., Bretherton, C. S., Marchand, R., Protat, A., DeMott, P. J., Alexander, S., Rintoul, S. R., Roberts, G. C., Twohy, C. H., Toohey, D. W., et al.: Airborne, ship- and ground-based observations of clouds, aerosols and precipitation from recent field projects over the Southern Ocean, in: Proceedings of the AGU Fall Meeting, Washington, D.C., USA, 10-14 December 2018, A53D-06, 2018.

McFarquhar, G. M., Bretherton, C. S., Marchand, R., Protat, A., DeMott, P. J., Alexander, S. P., Roberts, G. C., Twohy, C. H., Toohey, D., Siems, S., et al.: Observations of clouds, aerosols, precipitation, and surface radiation over the Southern Ocean: An overview of CAPRICORN, MARCUS, MICRE, and SOCRATES, Bulletin of the American Meteorological Society, 102(4), E894–E928, https://doi.org/10.1175/BAMS-D-20-0132.1, 2021.

McGill, M., Hlavka, D., Hart, W., Scott, V. S., Spinhirne, J., & Schmid, B.: Cloud physics lidar: Instrument description and initial measurement results, Applied Optics, 41(18), 3725–3734, https://doi.org/10.1364/AO.41.003725, 2002.

NCAR/EOL HSRL Team: Gulfstream V High Spectral Resolution Lidar (GV-HSRL), UCAR/NCAR - Earth Observing Laboratory [data set], https://doi.org/10.5065/d67w6976, 2012.

NCAR/EOL HCR Team: HIAPER Cloud Radar (HCR), UCAR/NCAR - Earth Observing Laboratory [data set], https://doi.org/10.5065/D6BP00TP, 2014.

NCAR/EOL HCR Team, NCAR/EOL HSRL Team: SOCRATES: NCAR HCR radar and HSRL lidar moments data. Version 3.2, UCAR/NCAR - Earth Observing Laboratory [data set], https://doi.org/10.5065/D64J0CZS, 2023.

https://doi.org/10.5194/amt-2024-124
Preprint. Discussion started: 5 August 2024

Atmospheric Measurement Techniques
Discussions

Oh, S.-B., Lee, Y. H., Jeong, J.-H., Kim, Y.-H., and Joo, S.: Estimation of the liquid water content and Z–LWC relationship using Ka-band cloud radar and a microwave radiometer, Meteorological Applications, 25, 423–434, https://doi.org/10.1002/met.1710, 2018.

Qiu, S., Dong, X., Xi, B., and Li, J.-L.F.: Characterizing Arctic mixed-phase cloud structure and its relationship with humidity and temperature inversion using ARM NSA observations, Journal of Geophysical Research: Atmospheres, 120, 7737–7746, https://doi.org/10.1002/2014JD023022, 2015.

Romatschke, U., Dixon, M., Tsai, P., Loew, E., Vivekanandan, J., Emmett, J., and Rilling, R.: The NCAR Airborne 94-GHz Cloud Radar: Calibration and Data Processing, Data, 6, 66, https://doi.org/10.3390/data6060066, 2021.

Romatschke, U., and Vivekanandan, J.: Cloud and precipitation particle identification using cloud radar and lidar measurements: Retrieval technique and validation, Earth and Space Science, 9, e2022EA002299, https://doi.org/10.1029/2022EA002299, 2022.

Sassen, K.: Deep Orographic Cloud Structure and Composition Derived from Comprehensive Remote Sensing Measurements, Journal of Climate and Applied Meteorology, 23, 568–583, http://www.jstor.org/stable/26181286, 1984.

Sassen, K.: The Polarization Lidar Technique for Cloud Research: A Review and Current Assessment, Bulletin of the American Meteorological Society, 72, 1848–1866, http://www.jstor.org/stable/26228894, 1991.

Schima, J., McFarquhar, G., Romatschke, U., Vivekanandan, J., D'Alessandro, J., Haggerty, J., et al.: Characterization of Southern Ocean Boundary Layer Clouds using airborne radar, lidar, and in situ cloud data: Results from SOCRATES, Journal of Geophysical Research: Atmospheres, 127, e2022JD037277, https://doi.org/10.1029/2022JD037277, 2022.

Scott, R. D., Krehbiel, P. R., and Rison, W.: The Use of Simultaneous Horizontal and Vertical Transmissions for Dual-Polarization Radar Meteorological Observations, Journal of Atmospheric and Oceanic Technology, 18, 629–648 https://doi.org/10.1175/1520-0426(2001)018<0629:TUOSHA>2.0.CO;2, 2001.

Shupe, M. D., Uttal, T., and Matrosov, S. Y.: Arctic Cloud Microphysics Retrievals from Surface-Based Remote Sensors at SHEBA, Journal of Applied Meteorology and Climatology, 44, 1544–1562, https://doi.org/10.1175/JAM2297.1, 2005.

Shupe, M. D.: A ground-based multisensor cloud phase classifier, Geophysical Research Letters, 34, L22809, https://doi.org/10.1029/2007GL031008, 2007.

Trenberth, K. E., and Fasullo, J. T.: Simulation of present-day and twenty-first-century energy budgets of the Southern Oceans, Journal of Climate, 23, 440–454, https://doi.org/10.1175/2009JCLI3152.1, 2010.

UCAR/NCAR - Earth Observing Laboratory: NSF/NCAR GV HIAPER Raw 2D-S Imagery. Version 1.1, UCAR/NCAR - Earth Observing Laboratory [data set], https://doi.org/10.26023/9555-DKY0-J604, 2018.

Uetake, J., Hill, T. C. J., Moore, K. A., DeMott, P. J., Protat, A., and Kreidenweis, S. M.: Airborne bacteria confirm the pristine nature of the Southern Ocean boundary layer, Proceedings of the National Academy of Sciences, 117, 13275–13282, https://doi.org/10.1073/pnas.2000134117, 2020.

https://doi.org/10.5194/amt-2024-124
Preprint. Discussion started: 5 August 2024

Vivekanandan, J., Ellis, S., Tsai, P., Loew, E., Lee, W.-C., Emmett, J., et al.: A wing pod-based millimeter wavelength airborne cloud radar, Geoscientific Instrumentation, Methods and Data Systems, 4, 161–176, https://doi.org/10.5194/gi-4-161-2015, 2015.

Vivekanandan, J., Ghate, V. P., Jensen, J. B., Ellis, S. M., and Schwartz, M. C.: A Technique for Estimating Liquid Droplet Diameter and Liquid Water Content in Stratocumulus Clouds Using Radar and Lidar Measurements, Journal of Atmospheric and Oceanic Technology, 37, 2145–2161, https://doi.org/10.1175/JTECH-D-19-0092.1, 2020.

Wang, Y., Zhang, D., Liu, X., and Wang, Z.: Distinct contributions of ice nucleation, large-scale environment, and shallow cumulus detrainment to cloud phase partitioning with NCAR CAM5, Journal of Geophysical Research: Atmospheres, 123, 1132–1154, https://doi.org/10.1002/2017JD027213, 2018.

Wang, Z., and Sassen, K.: Cloud Type and Macrophysical Property Retrieval Using Multiple Remote Sensors, Journal of Applied Meteorology, 40, 1665–1682, https://doi.org/10.1175/1520-0450(2001)040<1665>2.0.CO;2, 2001.

Wang, Z., Wechsler, P., Kuestner, W., French, J., Rodi, A., Glover, B., Burkhart, M., and Lukens, D.: Wyoming Cloud Lidar: instrument description and applications, Optics Express, 17, 13576–13587, https://doi.org/10.1364/OE.17.013576, 2009.

Wang, Z., French, J., Vali, G., Wechsler, P., Haimov, S., Rodi, A., Deng, M., Leon, D., Snider, J., Peng, L., and Pazmany, A. L.: Single Aircraft Integration of Remote Sensing and In Situ Sampling for the Study of Cloud Microphysics and Dynamics, Bulletin of the American Meteorological Society, 93, 653–668, https://doi.org/10.1175/BAMS-D-11-00044.1, 2012.

Wu, P., Dong, X., and Xi, B.: A Climatology of Marine Boundary Layer Cloud and Drizzle Properties Derived from Ground-Based Observations over the Azores, Journal of Climate, 33, 10133–10148, https://doi.org/10.1175/JCLI-D-20-0272.1, 2020.

Wu, P., Dong, X., Xi, B., Tian, J., and Ward, D. M.: Profiles of MBL cloud and drizzle microphysical properties retrieved from ground-based observations and validated by aircraft in situ measurements over the Azores, Journal of Geophysical Research: Atmospheres, 125, e2019JD032205, https://doi.org/10.1029/2019JD032205, 2020.

Wu, W., and McFarquhar, G.: NSF/NCAR GV HIAPER 2D-S Particle Size Distribution (PSD) Product Data. Version 1.1, UCAR/NCAR - Earth Observing Laboratory, https://doi.org/10.26023/8HMG-WQP3-XA0X, 2019.

Wu, W., and McFarquhar, G. M.: On the Impacts of Different Definitions of Maximum Dimension for Nonspherical Particles Recorded by 2D Imaging Probes, Journal of Atmospheric and Oceanic Technology, 33, 1057–1072, https://doi.org/10.1175/JTECH-D-15-0177.1, 2016.

Xi, B., Dong, X., Minnis, P., and Khaiyer, M. M.: A 10 year climatology of cloud fraction and vertical distribution derived from both surface and GOES observations over the DOE ARM SPG site, Journal of Geophysical Research, 115, D12124, https://doi.org/10.1029/2009JD012800, 2010.

Xi, B., Dong, X., Zheng, X., and Wu, P.: Cloud phase and macrophysical properties over the Southern Ocean during the MARCUS field campaign, Atmospheric Measurement Techniques, 15, 3761–3777, https://doi.org/10.5194/amt-15-3761-2022, 2022.

https://doi.org/10.5194/amt-2024-124
Preprint. Discussion started: 5 August 2024

Atmospheric Measurement Techniques Discussions

Zaremba, T. J., Rauber, R. M., McFarquhar, G. M., Hayman, M., Finlon, J. A., and Stechman, D. M.: Phase characterization of cold sector Southern Ocean Cloud tops: Results from SOCRATES, Journal of Geophysical Research: Atmospheres, 125, e2020JD033673, https://doi.org/10.1029/2020JD033673, 2020.

Zhao, L., Zhao, C., Wang, Y., Wang, Y., and Yang, Y.: Evaluation of cloud microphysical properties derived from MODIS and Himawari-8 using in situ aircraft measurements over the Southern Ocean, Earth and Space Science, 7, e2020EA001137, https://doi.org/10.1029/2020EA001137, 2020.

Zhao, X., Liu, X., Burrows, S., DeMott, P. J., Diao, M., McFarquhar, G. M., Patade, S., Phillips, V., Roberts, G. C., Sanchez, K. J., et al.: Important ice processes are missed by the Community Earth system model in Southern Ocean mixed-phase clouds: Bridging SOCRATES observations to model developments, Journal of Geophysical Research: Atmospheres, 128, e2022JD037513, https://doi.org/10.1029/2022JD037513, 2023.

Zheng, X., Dong, X., Xi, B., Logan, T., and Wang, Y.: Distinctive aerosol-cloud-precipitation interactions in marine boundary layer clouds from the ACE-ENA and SOCRATES aircraft field campaigns, EGUsphere, 2023, 1–45, https://doi.org/10.5194/egusphere-2023-2608, 2023.